Title
Formation of Fully Stoichiometric, Oxidation-State Pure Neptunium and Plutonium Dioxides from Molecular Precursors

Journal
Inorganic Chemistry, 63(39)

ISSN
0020-1669

Authors
Peterson, Appie
Kelly, Sheridon N
Arino, Trevor
et al.

Publication Date
2024-09-30

DOI
10.1021/acs.inorgchem.4c02099

Peer reviewed

Inorganic Chemistry

pubs.acs.org/IC
Article

Formation of Fully Stoichiometric, Oxidation-State Pure Neptunium and Plutonium Dioxides from Molecular Precursors

Appie Peterson, Sheridon N. Kelly, Trevor Arino, S. Olivia Gunther, Erik T. Ouellette, Jennifer N. Wacker, Joshua J. Woods, Simon J. Teat, Wayne W. Lukens, John Arnold,* Rebecca J. Abergel,* and Stefan G. Minasian*

Cite This: *Inorg. Chem.* 2024, 63, 18417−18428

Read Online

ACCESS | Metrics & More | Article Recommendations | Supporting Information

ABSTRACT: Amidate-based ligands (*N*-(*tert*-butyl)isobutyramide, **ITA**) bind κ^2 to form homoleptic, 8-coordinate complexes with tetravalent ^{237}Np (Np(ITA)$_4$, **1-Np**) and ^{242}Pu (Pu(ITA)$_4$, **1-Pu**). These compounds complete an isostructural series from Th, U−Pu and allow for the direct comparison between many of the early actinides with stable tetravalent oxidation states by nuclear magnetic resonance (NMR) spectroscopy and single crystal X-ray diffraction (SCXRD). The molecular precursors are subjected to controlled thermolysis under mild conditions with the exclusion of exogenous air and moisture, facilitating the removal of the volatile organic ligands and ligand byproducts. The preformed metal−oxygen bond in the precursor, as well as the metal oxidation state, are maintained through the decomposition, forming fully stoichiometric, oxidation-state pure NpO_2 and PuO_2. Powder X-ray diffraction (PXRD), scanning transmission electron microscopy (STEM), and energy dispersive X-ray spectroscopy (EDS) elemental mapping supported the evaluation of these high-purity materials. This chemistry is applicable to a wide range of metals, including actinides, with accessible tetravalent oxidation states, and provides a consistent route to analytical standards of importance to the field of nuclear nonproliferation, forensics, and fundamental studies.

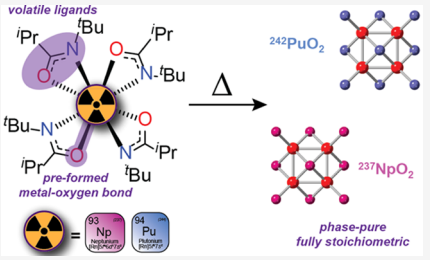

INTRODUCTION

Contemporary investments in nuclear reactors have the potential to supplant our global dependence on fossil fuels, increasing demand for fissile nuclear materials such as UO_2, PuO_2, and NpO_2, which are key components and byproducts of the nuclear fuel cycle.[1] The consequent need for innovation in applied nuclear materials necessitates increased investigation into the fundamental chemistry of the actinides. Despite this growing need, there are many open questions about the coordination chemistry, oxidation behavior, and material properties of these relevant fissile elements, which must be addressed to enable technological and policy advances.[2−4]

Recent innovations in nuclear forensics, analytical chemistry, and inorganic chemistry have provided a suite of techniques that can be used to identify the composition, history, and environmental impact of various nuclear materials.[4−9] Advances in microanalytical techniques have allowed for the identification of nanomolar quantities of fissile or fissionable nuclei of interest.[4,5,10,11] These techniques have enabled studies of the fundamental electronic structure, chemical behavior, and bonding nature of actinide oxides—often, with synthetic and computational efforts working in concert to describe the complicated chemistry of these materials.[12−19] However, for these studies to deliver reliable information—especially from a synthetic approach—a robust library of spectroscopically pure actinide dioxide (AnO_2) standards is needed.

Tetravalent dioxide materials are often used in fundamental investigations of electronic structure and bonding across the actinide series, necessitating pure and well-characterized material in order to make meaningful conclusions. Often methods to prepare such materials involve multiple steps of sintering under high pressures, calcination at elevated temperatures, and long annealing times (Figure 1a,b).[20−24] These syntheses are sensitive to the presence of oxygen, which can result in the formation of sub- or superstoichiometric oxides.[20,25−28] This is problematic for Pu, which is notorious for its tendency to form superstoichiometric (AnO_{2+x}) oxides.[20,25,26] Additionally, U, Np, and Pu can all access a wide range of oxidation states, presenting a challenge in the preparation of oxidation-state pure materials.[29] The extreme conditions currently employed to avoid the formation of nonstoichiometric dioxides often require specialized equipment and bespoke reaction vessels, raising safety concerns regarding pressurized reactive gases and radiological materials, while ultimately producing materials with irregular particle sizes, nonuniform morphologies, and other characteristics that

Received: May 21, 2024
Revised: August 23, 2024
Accepted: August 28, 2024
Published: September 16, 2024

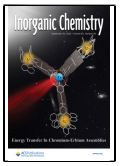

https://doi.org/10.1021/acs.inorgchem.4c02099
Inorg. Chem. 2024, 63, 18417−18428

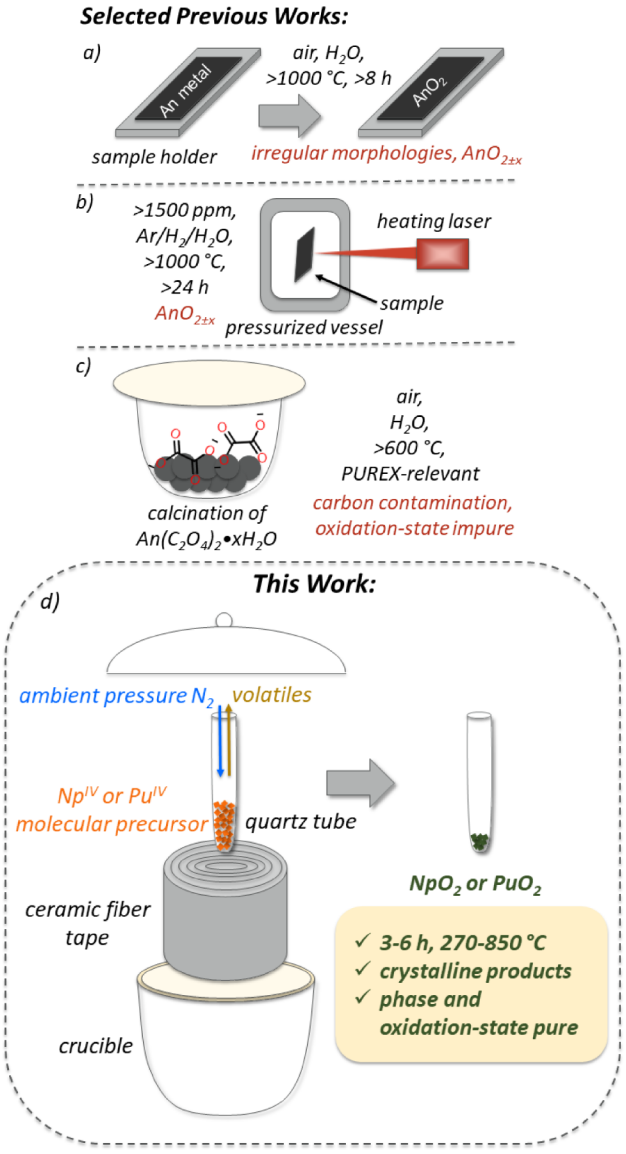

Figure 1. Selected methods for the preparation of actinide dioxides (An = actinide) by (a) firing metal (often stabilized by Ga or Se) in humid air,[20] adapted with permission from ref[20], Copyright Elsevier 2011, (b) laser-induced heating of actinide oxide powder in a pressurized vessel,[21] and (c) precipitation of actinide oxalate followed by calcination.[22,23,34] (d) This work.

do not meet the sample requirements for some spectroscopic studies.[24,30−32]

Alternatively, a simpler preparation of PuO_2 entails precipitation of Pu oxalate followed by calcination (Figure 1c)—a method that is ubiquitous due to its relatively mild conditions.[18,23,30,33−38] Despite the relative ease of this synthesis, the quality of the resulting actinide oxide is highly variable with changes in reaction conditions (e.g., concentration of oxalate, rate of addition, calcination temperature, presence of impurities due to sample history).[4,18,33−35,39] The lack of oxidation-state control introduced by calcination in air and residual organic contamination from ligands makes this method suboptimal for the consistent preparation of high-purity PuO_2 materials.

In addition to challenges with chemical purity and crystallinity, most conventional synthetic methods are unable to control the dimensionality of AnO_2 materials, and are thus poorly suited to the preparation of thin films and multilayer heterostructures.[40] Atomically precise, crystalline thin films are needed for experimental studies of AnO_2 surface chemistry, and to support the development of computational models of AnO_2 corrosion during long-term storage.[15,41−43] A novel solution-based technique was recently developed for synthesizing high-quality epitaxial thin films of actinide materials, including carbides, nitrides, and oxides.[44] Their approach enabled the first measurement of the optical band gap for NpO_2 and PuO_2, which is a crucial value for the validation of the computational methods used to predict the properties of transuranic materials.[45] Chemical vapor deposition (CVD) is another promising approach, and volatile lanthanide and U complexes have been developed as precursors for the CVD of thin films.[46−48] However, precursors with the requisite volatility, thermal stability, and a suitable pathway for clean decomposition have not been developed for the transuranic elements.

To this end, we recently reported tetravalent Th and U molecular coordination complexes $Th(ITA)_4$ and $U(ITA)_4$ (**ITA** = *N*-(*tert*-butyl)isobutyramide, Figure S1) and studied their viability as molecular precursors.[49,50] Pyrolysis and NMR spectroscopic characterization of the decomposition byproducts showed that the complexes undergo alkene elimination to yield ThO_2 and UO_2 without the need for an external oxygen source. The purity of the oxide products was sensitive to the precursor ligand substituents, with higher-purity products resulting from more volatile ligands and ligand byproducts; ThO_2 formed by thermal decomposition of $Th(ITA)_4$ was of higher purity and crystallinity than ThO_2 samples formed by decomposition of aryl-substituted amidate ligands.[49] The Th complex sublimed cleanly at atmospheric pressure and elevated temperature, and CVD on silicon using $U(ITA)_4$ as a molecular precursor at reduced pressure resulted in epitaxial growth of a highly crystalline UO_2 thin film with thickness of ca. 400 nm.[49]

Encouraged by these results with Th and U, we sought to extend this chemistry to the transuranic elements Np and Pu. A widely applicable method for the preparation of high-purity NpO_2 and PuO_2 under mild conditions and without specialized reaction vessels would have broad implications for both theoretical and applied studies of the actinides.

Here, we report the preparation of the homoleptic coordination complexes $Np(ITA)_4$ and $Pu(ITA)_4$ and their spectroscopic and crystallographic comparison to the isostructural $Th(ITA)_4$ and $U(ITA)_4$ analogues. The synthetic route was designed to be readily scalable, sustainable, and broadly implementable. Subsequent thermolysis of the coordination complexes under inert conditions confirmed their utility as precursors to high-purity actinide dioxide materials. The method reported here provides access to high-purity samples of a notoriously complicated material, PuO_2, establishing a new, precursor-based route with mild reaction conditions to facilitate physical-inorganic characterization.

RESULTS AND DISCUSSION

Work with transuranic elements is kept to milligram-scale reactions due to considerations of limited availability and radiological safety, thus we first developed a reproducible and high-yielding synthetic route for $U(ITA)_4$ (**1-U**) with the lower specific activity isotope ^{238}U, before application to $Np(ITA)_4$ (**1-Np**) and $Pu(ITA)_4$ (**1-Pu**, Figure 2). This

https://doi.org/10.1021/acs.inorgchem.4c02099
Inorg. Chem. 2024, 63, 18417−18428

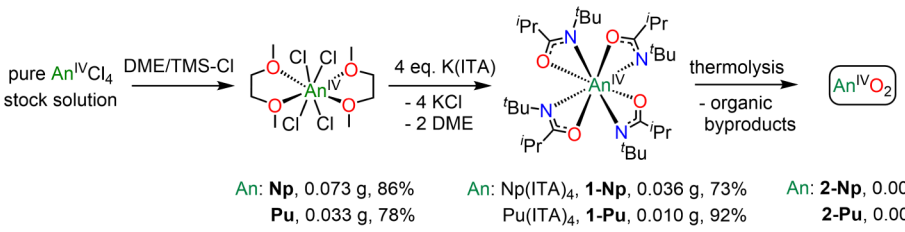

Figure 2. Synthetic route to **1-Np** (Np(ITA)$_4$) and **1-Pu** (Pu(ITA)$_4$), and their thermolysis products **2-Np** (NpO_2) and **2-Pu** (PuO_2).

compound (**1-U**) was chosen as a model system for ^{237}Np and ^{242}Pu due to the relatively close match in ionic radii and accessibility of a comparable range of oxidation states.[29] The relevance of U as a model system for Np and Pu is due in part to the similar relative energies of the frontier orbitals of the tetravalent ions—5f^2, 5f^3, and 5f^4—for U^{IV}, Np^{IV}, and Pu^{IV}, respectively.[29]

Toward the preparation of inert transuranic starting materials, stock solutions of ^{237}Np and ^{242}Pu were separately obtained from the residues of previous spent synthetic reactions by digestion in HNO_3 followed by a series of bulk precipitations using HF and NH_4OH (see "Radiochemical Purifications and Separations" in Supporting Information).[51−53] Oxidation-state (characterized by UV−vis−NIR spectroscopy, Figure S2) and radiochemically pure (confirmed by liquid scintillation counting, γ-spectroscopy, and α-spectroscopy, Figures S3−S5) tetravalent ^{237}Np was obtained as a chloride stock solution in HCl, following reduction with NH_2OH_2·HCl and separation from its radiochemical daughters (^{233}Pa, ^{233}U) via anion exchange chromatography. Similarly, purified tetravalent ^{242}Pu was obtained as a chloride stock solution in HCl (Figures S6 and S7) after anion exchange chromatographic separation of the ^{241}Am daughter that grew in due to the radioactive decay of a small amount of ^{241}Pu (≪0.001 wt %) in the legacy material available at Lawrence Berkeley National Laboratory (LBNL).

Following a modified reported procedure, the proligand, **H(ITA)**, was prepared by straightforward amide coupling of *tert*-butylamine with isobutyryl chloride in diethyl ether.[54] Notably, purification of the final product by extraction rather than sublimation was more efficient.[49,54,55] Treating **H(ITA)** with a slight excess of potassium bis(trimethylsilyl)amide (KHMDS) in toluene provided the potassium salt, **K(ITA)**, which was isolated in high purity and excellent yield. The total combined yield for the preparation of **K(ITA)** was 87% and could be achieved on a multigram scale. The homoleptic amidate complexes Np(ITA)$_4$ (**1-Np**, 0.036 g, 73%) and Pu(ITA)$_4$ (**1-Pu**, 0.010 g, 92%) were prepared via salt metathesis of **K(ITA)** with **NpCl$_4$(DME)$_2$** and **PuCl$_4$(DME)$_2$** in dimethoxyethane (DME), respectively.

Multiple coordination numbers and geometries could be anticipated for **1-Np** and **1-Pu** because amidate ligands can adopt several distinct binding modes.[49,56,57] For example, the amidate proligand *N-tert*-butylpivalamide (TTA) has a comparable steric profile to that of ITA, differing by the presence of a *tert*-butyl or an iso-propyl group on the backbone. However, **1-U** adopts an 8-coordinate geometry with all four ITA ligands chelated in a (κ^2-O,N) fashion, whereas U(TTA)$_4$ has two TTA ligands chelated κ^2-O,N and two bound only through the oxygen atom, κ^1-O. In the case of **1-Np** and **1-Pu**, the ^{1}H NMR spectra both displayed three resonances (Figures S8 and S10) that were readily assigned to the isopropyl methine, isopropyl methyl, and *tert*-butyl protons using 2D NMR (Figures S9 and S11). In this regard, the ^{1}H NMR spectra of **1-Np** and **1-Pu** resembled those of **1-Th** and **1-U** (Figure S12),[49] which suggests that all four complexes adopt the same 8-coordinate geometry with four ITA ligands chelated (κ^2-O,N) to the metal center in the solution phase.

UV−vis−NIR spectra of **1-Np** and **1-Pu** were measured from isolated crystals redissolved in Et_2O and compared to those of the precursors **NpCl$_4$(DME)$_2$** and **PuCl$_4$(DME)$_2$** and **H(ITA)** (Figures S13−S16). Sharp features associated with 5f → 5f transitions in **1-Np** (Figures 3 and S16) arise at 13,812

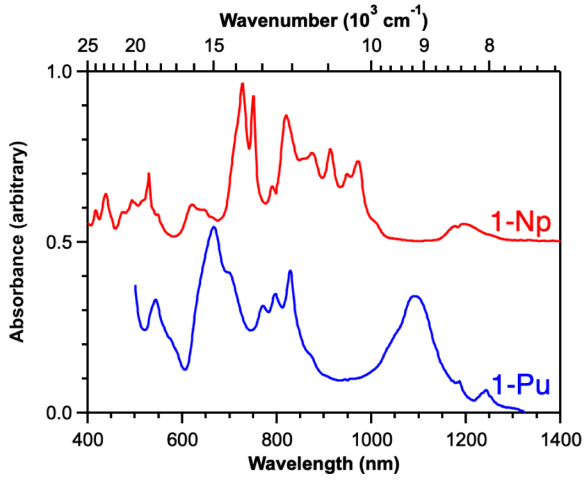

Figure 3. Solution phase UV−vis−NIR stacked plot of **1-Np** (top, red) and **1-Pu** (bottom, blue) in Et_2O.

cm^{-1} (724 nm) and 10,416 cm^{-1} (960 nm), and are likely attributable to $^4I_{9/2} \rightarrow {}^4F_{3/2}$ and $^4I_{9/2} \rightarrow {}^4I_{13/2}$, respectively.[58] These features can also be identified in the spectra obtained for the tetravalent Np starting materials (Figure S17), with slight shifts (±5 nm) ascribed to variations in solvents and coordination environment of the metal center. Several intense, sharp features are present between 10,000 and 14,000 cm^{-1}. The large quantity of sharp features is consistent with observations made for comparable systems with κ^2-O,N ligands like Np^{IV}(^{Ar}acnac)$_4$[59] and Np^{IV}[(^{t}BuNO)py]$_4$,[60] and are likely attributable to well-resolved 5f → 5f transitions, though their specific assignment requires theoretical investigation of the particular transitions in organic media. Broader features (15,527 cm^{-1}, ε = 13 M^{-1} cm^{-1}; 16,181 cm^{-1}, ε = 15 M^{-1} cm^{-1}; 18,181 cm^{-1}, ε = 11 M^{-1} cm^{-1}; 18,867 cm^{-1}, ε = 28 M^{-1} cm^{-1}; 20,325 cm^{-1}, ε = 17 M^{-1} cm^{-1}; 21,321 cm^{-1}, ε = 12 M^{-1} cm^{-1}; 22,779 cm^{-1}, ε = 20 M^{-1} cm^{-1}; 23,923 cm^{-1}, ε = 13 M^{-1} cm^{-1}) are present in the higher energy range of the spectrum (15,000−24,000 cm^{-1}) and are comparable to those identified for **NpCl$_4$(DME)$_2$**.[61,62] In the solution-phase UV−vis−NIR spectrum of **1-Pu** (Figures 3 and S18), broad features

https://doi.org/10.1021/acs.inorgchem.4c02099
Inorg. Chem. 2024, 63, 18417−18428

associated with characteristic Pu^{IV} appear at 18,416 cm^{-1} (543 nm, $^5I_4 \rightarrow {}^5F_3$) and 8779 cm^{-1} (1139 nm, $^5I_4 \rightarrow {}^5I_6$), consistent with those present for $PuCl_4(DME)_2$ (Figure S19). Between 10,000 and 13,000 cm^{-1}, three sharp, low-intensity features (12,048 cm^{-1}, ε = 17 M^{-1} cm^{-1}; 12,547 cm^{-1}, ε = 15 M^{-1} cm^{-1}; 12,953 cm^{-1}, ε = 13 M^{-1} cm^{-1}) are identified and, similarly to **1-Np**, are attributed to 5f → 5f transitions.

X-ray crystal structures of **1-Np** and **1-Pu** (Figure 4) were obtained to evaluate whether the solid-state geometry was in

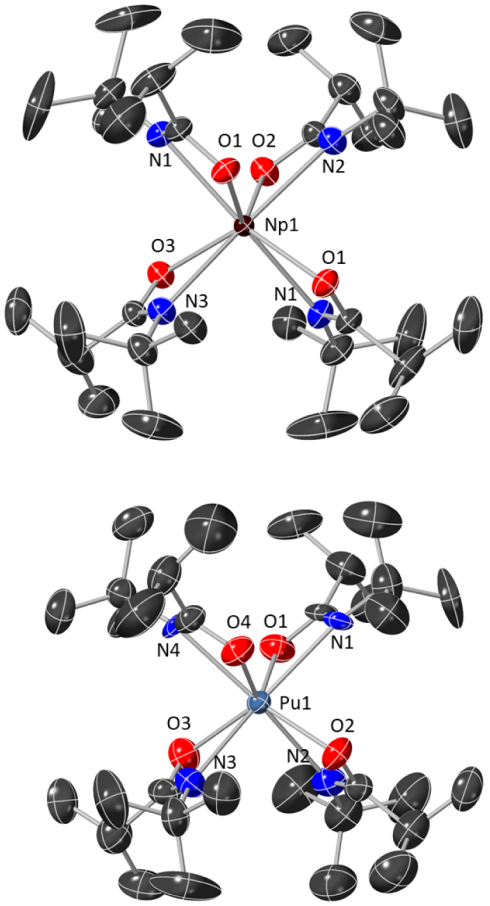

Figure 4. Structures of **1-Np** (top) and **1-Pu** (bottom). Both structures are represented with 50% probability thermal ellipsoids at 100 K and have hydrogen atoms omitted for clarity.

agreement with that observed by solution-phase NMR spectroscopy. Diffraction-quality single crystals of **1-Np** and **1-Pu** were grown from concentrated solutions in Et_2O at −35 °C and mounted via established containment methods for transuranic samples.[63] **1-Np** crystallizes in a base-centered, orthorhombic space group ($Cmc2_1$), while **1-Pu** crystallizes in a centrosymmetric, base-centered monoclinic space group $P2_1/n$, which is consistent with the **1-Th** and **1-U** congeners. **1-Np** refined well with a unit cell of $Cmc2_1$ symmetry, but could not be refined in $P2_1/n$. This discrepancy may be a consequence of disparate N_2 or solvent molecules in the lattice that were not modeled. The structures are 8-coordinate, with four ITA ligands each bound κ^2-O,N to the respective metal center in a square antiprismatic geometry. The average An−N distance is slightly longer than the average An−O distance for both **1-Np** and **1-Pu** (Table 1, 0.147(2) Å longer and 0.165(3) Å longer, respectively). This trend is consistent with those observed for

Table 1. Selected metrics and average metal−ligand bond lengths for 1-Np and 1-Pu

	1-Np	1-Pu
space group	$Cmc2_1$	$P2_1/n$
R_1 (w/R_2)	0.0328(0.0614)	0.0335(0.0983)
Ave. M−O (Å)[a]	2.325(3)	2.310(4)
Ave. M−N (Å)[a]	2.472(4)	2.475(5)

[a]Standard error of the mean given in parentheses in the same units as the final digit.

the isostructural compounds (**1-Th** and **1-U**) and likely due to multiple factors including stronger An−O ionic bonding resulting from localization of electron density on the O atom and the smaller ionic radius of O relative to N.[49,50] Overall, the average metal−ligand interatomic distances decrease as expected when moving along the actinide series: **1-Th** > **1-U** > **1-Np** > **1-Pu** (Tables 1, S1, and Figure S20).[29]

On average, the Np−O distance is consistent with those reported for comparable Np^{IV} coordination complexes (2.3−2.5 Å).[52,64−78] Similarly, the average Np−N distance is well within the expected range (2.4−2.6 Å) for 8-coordinate Np^{IV} structures.[66,68,70,71,73,79] For **1-Pu**, the average Pu−O (2.310(4) Å) and Pu−N (2.475(5) Å) distances are also consistent with expectations based on previous reports: Pu−O: 2.2−2.5 Å,[59,60,68,71,77,80−83] Pu−N: 2.4−2.6 Å.[59,60,68,71,77,79,84] The Pu−O distance is 0.016(2) Å shorter than the Np−O distance, which is consistent with the expected bond contraction observed due to a systematic contraction of the metal radii.[85] On the other hand, the Pu−N distance is statistically equivalent to the Np−N distance, and the likelihood that this difference is due to variance is less than 5%.

With **1-Np** and **1-Pu** in hand, we proceeded with the thermolysis of each sample under inert conditions comparable to those reported for **1-Th** and **1-U** (N_2).[49,50] In accordance with previous reports of molecular precursors to oxide materials,[49,50,55] we hypothesized that the mechanism for thermolysis of **1-Np** and **1-Pu** would be analogous to the mechanism determined previously for **1-Th** and **1-U** by observation of the decomposition byproducts isobutylene, isobutyronitrile and H(ITA) upon formation of ThO_2 and UO_2 (Figure S1).[50] These expected decomposition products are particular to the ITA ligand system,[49,50,55] selected in part for the volatility inherent to the ligand itself as well as it is decomposition byproducts, presumably allowing the efficient removal of residual organics from the final oxide product. Importantly, under an inert atmosphere the oxygen in the final product would be present from the preformed M−O bonds in the precursor, allowing for stoichiometric control of the resulting oxides. Thermolysis experiments were performed inside an inert atmosphere glovebox using a muffle furnace. Isolated crystals of **1-Np** and **1-Pu** were loaded into quartz tubes with openings to permit evaporation and removal of organic byproducts into the glovebox atmosphere (see Figure 1d for experimental diagram). Thermolysis experiments were performed at 270 °C (temperature selected based on previous thermogravimetric measurements with U[49] and optionally subjected to an additional annealing step at 850 °C (see Table S2 for details).

Thermolysis of **1-Np** at 270 °C produced a mustard-yellow powder (**2a-Np**), and incorporation of the optional annealing step at 850 °C resulted in a dark green crystalline powder (**2b-Np**). For **1-Pu**, thermolysis at 270 °C resulted in an olive-

https://doi.org/10.1021/acs.inorgchem.4c02099
Inorg. Chem. 2024, 63, 18417−18428

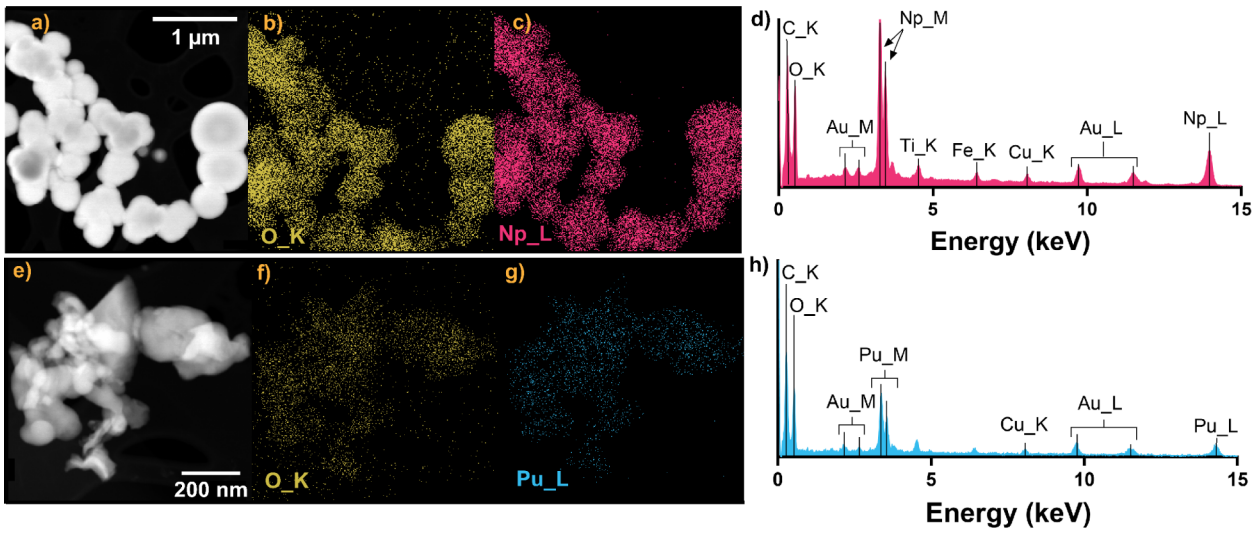

Figure 5. High-angle annular dark field (HAADF) scanning transmission electron microscopy (STEM) images of NpO_2 (**2a-Np**, a) and PuO_2 (**2a-Pu**, e) were prepared from **1-Np** and **1-Pu** at 270 °C, respectively. Energy dispersive X-ray spectroscopy (EDS) elemental maps of oxygen (b and f) or actinide (Np, c and Pu, g) with the corresponding spectra (Np, d and Pu, h). Note, Au, Ti, Fe, Cu and C are all present in the tomography tip, specimen holder, and TEM grids.

green powder (**2a-Pu**), and annealing at 850 °C produced a black crystalline powder (**2b-Pu**). Mass losses of between 63 and 71% were observed upon weighing, which are close to the predicted reduction in mass for complete decomposition of **1-Np** and **1-Pu**, formation of NpO_2 and PuO_2, and elimination of all ligand and ligand decomposition byproducts (ca. 66%).

High-angle annular dark-field scanning transmission electron microscopy (HAADF-STEM) was used to evaluate the nanoscale morphology and chemical composition of the thermolysis products (Figures 5 and S29–S36). The images show multiple particle morphologies in all four samples, including well-isolated ∼10 nm crystallites and >500 nm microspheres. All four samples were analyzed by energy dispersive X-ray spectroscopy (EDS) elemental mapping to evaluate chemical purity and stoichiometry (Figures S29–S36, Tables S4–S7). The presence of trace C impurities could not be reliably determined given the lacy carbon TEM grids used for sample mounting. However, no N was detected, which suggests full decomposition of the precursors and elimination of the expected organic byproducts. The O weight percentages determined for each sample are close to the predicted values of 13.5 and 13.2% for NpO_2 and PuO_2, respectively (Tables S4–S7).

Powder X-ray diffraction (PXRD) was used to determine the crystallinity and phase purity of the annealed thermolysis products. The experimental PXRD patterns for samples **2b-Np** and **2b-Pu** were assigned as NpO_2 (**2b-Np**, Figure 6, top) and PuO_2 (**2b-Pu**, Figure 6, bottom), and are in excellent agreement with the corresponding calculated powder patterns, matching in terms of number of reflections, reflection intensities, and *d*-spacings.[86,87] Scherrer analysis (using reflections (111) and (200) for each pattern) was applied to the powder patterns to determine crystallite sizes, which were 9.8 ± 0.13 and 9.7 ± 0.12 nm for **2b-Np** and **2b-Pu**, respectively, and in agreement with some particle sizes observed by STEM (Figures S33 and S35).[88,89] STEM imaging also revealed larger particle aggregates, which prohibited further quantitative particle size analysis toward understanding the size uniformity of the samples as well as the potential presence of amorphous oxide-based material (Figures S33 and S35). As line broadness increases with decreasing particle size, the small particle sizes calculated here are consistent with the observed broadness of the experimental powder patterns. This result was unexpected after annealing at

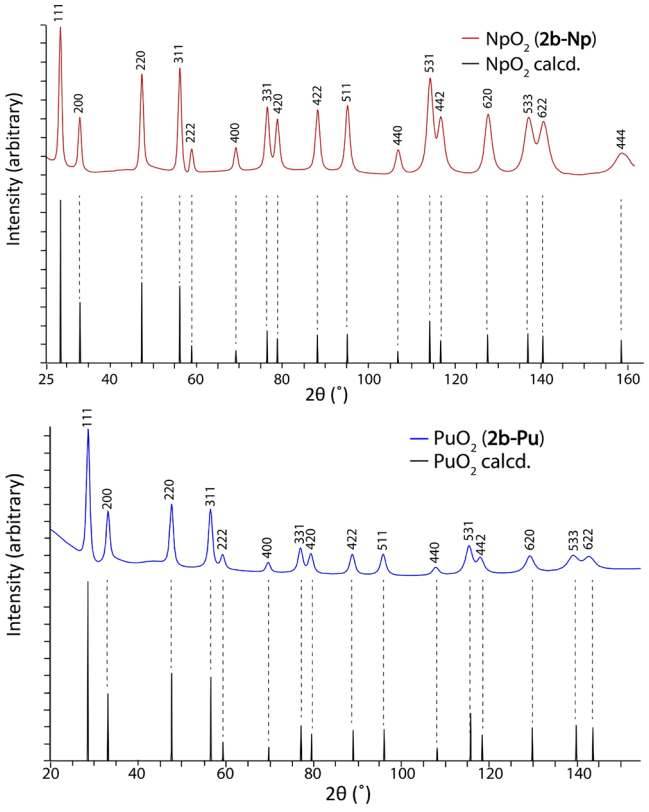

Figure 6. Powder X-ray diffraction patterns (PXRD) collected with Cu Kα radiation at room temperature for **2b-Np** (top, red, lattice constant = 5.431(5) Å) compared to calculated NpO_2 (top, black, ICSD: 647175),[86] and **2b-Pu** (bottom, blue, lattice constant = 5.395(5) Å) compared to calculated PuO_2 (bottom, black, ICSD: 186183).[87].

https://doi.org/10.1021/acs.inorgchem.4c02099
Inorg. Chem. 2024, 63, 18417−18428

850 °C, which is known to increase particle size for traditionally calcinated transuranic samples (214 ± 81 nm).[24,30]

A critical question was whether the samples of **2b-Np** or **2b-Pu** were best described as stoichiometric NpO_2 and PuO_2, or if they contained significant components of nonstoichiometric oxide impurities. Finely divided actinide oxides are known to oxidize along grain boundaries, and a wide variety of binary and nonbinary oxides are known.[28,29,90] Previous work has shown that the lattice parameter for PuO_2 is very sensitive to minor impurities in metal oxidation state or material stoichiometry.[27,36] Larger parameters have been attributed to the presence of Pu^{III} (Pu_2O_3) or initial expansion of the lattice to accommodate interstitial O^{2-} (PuO_{2+x}).[27,36] In this work, the lattice parameters for the cubic space group $Fm\bar{3}m$ were $a = b = c = 5.431(5)$ Å (**2b-Np**) and 5.395(5) Å (**2b-Pu**). These experimentally determined values are in close agreement (**2b-Np**: 0.14% and **2b-Pu**: 0.03% error) with those most widely referenced for the fully stoichiometric dioxides ($NpO_{2.00}$ = 5.4241(3) Å and $PuO_{2.00}$ = 5.3975(1) Å),[27,91] indicating high phase- and oxidation-state purity.

SUMMARY AND CONCLUSION

Previously, it has been proposed that the highest quality PuO_2 could be obtained through the exclusion of air and moisture.[25] The results presented here confirm this hypothesis and provide a reliable method to prepare highly ordered NpO_2 and PuO_2 from molecular precursors under mild, inert conditions.

Characterization of the precursors **1-Np** and **1-Pu** using NMR spectroscopy and single-crystal X-ray diffraction showed that both have the same coordination number and geometry in solution and in the solid state, with all four of the ITA ligands chelated in a κ^2-O,N fashion. Isolation of **1-Np** and **1-Pu** completes an isostructural series of early tetravalent actinides with Th and U and allows for rare direct comparison of periodic trends from spectroscopic and structural characterization.[59,92−96]

The thermal decomposition of **1-Np** and **1-Pu** and annealing under inert conditions afforded NpO_2 and PuO_2. Lattice constants obtained by PXRD supported our formulation of the products as stoichiometric NpO_2 and PuO_2, and did not provide evidence for the formation of other binary or nonstoichiometric oxide phases. The observed mass loss and EDS measurements are consistent with clean conversion to the products without detectable remaining organic byproducts from the precursor ligands, notwithstanding the potential for trace remaining C, which cannot be ruled out at this time. Based on our previous studies of $Th(ITA)_4$ and $U(ITA)_4$, the stoichiometric control of the product is likely provided by the preformed metal−oxygen bond in the precursor, while the oxidation state of the metal is predetermined in the coordination complex and maintained throughout the thermolysis.

The fundamental chemistry of PuO_2 is complex and intensely debated, partly due to sample inconsistencies arising from subtle differences in synthetic preparation.[20,22,23,25,26,28,30,34,36,97] These inconsistencies can have significant negative consequences for efforts in nuclear forensics and nonproliferation, where detailed kinetic and thermodynamic models of PuO_2 aging are needed to evaluate the history and provenance of nuclear materials.[4,34,36,98]

Our molecular precursor-based approach is advantageous for future investigations of this critical material by providing synthetic samples of high-purity which are suitable for evaluation by a wide range of characterization techniques. In addition to the well-defined decomposition mechanism which leads to actinide dioxide products, the ITA ligand has been shown previously to impart thermal stability and volatility to precursor compounds, such that $Th(ITA)_4$ sublimed cleanly at atmospheric pressure and $U(ITA)_4$ sublimed at reduced pressure (10^{-6} mbar).[49,50] This quality supports the possible utility of $Np(ITA)_4$ and $Pu(ITA)_4$ in gas-phase synthesis methods such as CVD, atomic layer deposition (ALD), or in the formation of inorganic−organic hybrid materials under similar conditions to the U analogue.[15,49] In doing so, this work bolsters safeguards required in the fields of nuclear forensics and nonproliferation, and establishes a facile route to high-purity actinide dioxides for future studies of their fundamental bonding and reactivity.

EXPERIMENTAL SECTION

Materials and Instruments. Caution: The ^{237}Np ($t_{1/2} = 2.144 \times 10^6$ y)[99] and ^{242}Pu ($t_{1/2} = 3.75 \times 10^5$ y)[99] isotopes, and their decay daughters, emit α- and β-particles, as well as γ-radiation, all of which pose a significant risk to human health. **Note:** the ^{242}Pu stock is 99.98% ^{242}Pu by mass and is responsible for 84% of the α-particles emitted from the sample. A small (0.02% mass fraction) amount of ^{240}Pu ($t_{1/2} = 6.561 \times 10^3$ y)[99] and ^{238}Pu (<0.01% mass fraction, $t_{1/2}$ = 87.71 y)[99] are responsible for 16% of the α-particles emitted from the sample. A much smaller (≪0.001% mass fraction) amount of ^{241}Pu ($t_{1/2}$ = 14.329 y, β—99.998%)[99] does not contribute significantly to mass fraction or α-particle emission, but results in a measurable amount of ^{241}Am ($t_{1/2}$ = 432.6 y),[99] which must be separated before proceeding with synthetic efforts. The handling of said isotopes was conducted in a specialized radiation chemistry research facility—the Heavy Element Research Laboratory (HERL) at Lawrence Berkeley National Laboratory (LBNL)—equipped with high-efficiency particulate air (HEPA) filtered fume hoods and negative pressure (air or N_2-filled) gloveboxes. Safety measures such as appropriate personal protective equipment, body and extremity dosimetry, portable survey meters, and benchtop scalers were employed to ensure researcher safety and accurate isotope material tracking. Additionally, the entrance/exit of the HERL is equipped with a Canberra Sirius 5PAB hand-and-foot personal contamination monitoring station.

All aqueous stock solutions used in the preparation of radiochemically pure starting materials were prepared with Optima grade (Fisher Scientific) acids and bases (HCl, HF, HNO_3, NH_4OH) and Milli-Q water (18 MΩ·cm). ^{237}Np and ^{242}Pu were separated from their respective decay daughters employing AG MP-1 anion exchange resin (BioRad, chloride form, 50−100 mesh).

All reactions containing air- or water-sensitive compounds were performed within the inert atmosphere of a negative pressure N_2-filled MBraun glovebox. *tert*-Butylamine (98%) and triethylamine (≥99.5%) were purchased from Sigma-Aldrich, stored over 5 Å molecular sieves, and used without further purification. Isobutyryl chloride (98%) was purchased from VWR, dried over CaH_2 under an atmosphere of Ar, then degassed via three cycles of freeze−pump−thaw before purification by distillation. Potassium bis(trimethylsilyl)-amide (95%) was purchased from Sigma-Aldrich and recrystallized from toluene before use. All protonated solvents were degassed, passed through a solvent purification system (MBraun SPS-800), and tested with a dilute solution of Na_2Ph_2CO in THF before use. Anhydrous Et_2O, DME, toluene-d_8, *n*-hexane, and Me_3SiCl were dried over 5 Å molecular sieves, degassed via freeze−pump−thaw, and distilled before being stored under N_2.

Nuclear magnetic resonance (NMR) spectroscopy samples were prepared inside a negative pressure, N_2-filled glovebox by loading 200−250 μL of sample solution in toluene-d_8 into a precut (2.5 in) fluoroethylene propylene (FEP) liner (Wilmad 6005−7, O.D. 5 mm) and capped with a FEP stopper. The liner was then loaded into a screw cap NMR tube (VWR 76459−860), the threads of the NMR

https://doi.org/10.1021/acs.inorgchem.4c02099
Inorg. Chem. 2024, 63, 18417−18428

tube wrapped with Teflon tape before sealing with a screw cap. Samples were analyzed at 25 °C using either a Bruker AVANCE NEO 300 MHz spectrometer equipped with a 5 mm BBO probe or a Bruker AVANCE NEO 500 MHz spectrometer equipped with a PA 5 mm BBO probe. Chemical shifts for ^{1}H spectra were referenced to residual protium in the deuterated solvent (toluene-d_8) implementing the reference function in MestReNova (Mestrelab Research, S.L.). Solution phase UV−vis electronic absorption spectra were collected at ambient temperature using a Varian Cary 6000i UV−vis−NIR spectrophotometer (Agilent Technologies, Inc.) in 1 cm quartz cuvettes or a FLAME-T-XR1-ES spectrometer fitted with a CUV cuvette holder and a DH-2000 light source (Ocean Optics, Inc.) The spectrometer was controlled with OceanView software (Ocean Optics, Inc.).

Single crystal X-ray diffraction measurements were performed at the Advanced Light Source (ALS) of LBNL—Beamline 12.2.1, using a silicon double crystal monochromator to provide a beam of 17 keV (λ = 0.7288 Å) and the data sets collected at 100 K. At the time of publication, PLATON[100] did not have scattering factors for elements beyond uranium when nonstandard wavelengths are used, and therefore could not validate internally calculated $f'$and f'' values. Bruker APEX3 software was employed for data collection, scaling, and integration. Structure solutions were performed with SHELXT[101] and OLEX2[102] as graphical interface, and the structures were refined against F^2 on all data by full matrix least-squares with SHELXL.[103] Powder X-ray diffraction patterns were collected on a Rigaku Synergy-S diffractometer with a PhotonJet X-ray source and a HyPix-6000HE detector in "powder pattern" mode, using Cu Kα radiation (λ = 1.5406 Å). CrystalMaker 10 and CrystalDiffract 6.9.4 were used to render thermal ellipsoid plots of single crystal X-ray structures and stacked plots of calculated and experimental powder patterns, respectively.

Gamma (γ) spectroscopic measurements were performed on locally built high purity germanium (HPGe) detector with a 16 mm diameter, n-type HPGe crystal and an aluminum-coated Kevlar window. The detector was calibrated using a mixed isotope standard (^{241}Am, ^{109}Cd, ^{57}Co, ^{139}Ce, ^{203}Hg, ^{113}Sn, ^{137}Cs, ^{88}Y, ^{60}Co and ^{152}Eu) traceable to the National Institute of Standards and Technology and supplied by Eckert & Ziegler. All γ-spectroscopic measurements were controlled with GammaVision software (Ortec) and analyzed using Interspec, a spectral radiation analysis software from Sandia National Laboratory, which accounted for the detector efficiency based on the distance of the sample to the detector.[104] For ^{237}Np, the 86.4 keV peak with an absolute γ-ray emission probability (I_γ) of 0.122(3) was used in addition to the peaks at 86.6 keV (I_γ = 0.0201(7)), 300.1 keV (I_γ = 0.0654(8)), and 311.9 keV (I_γ = 0.382(5)) for the ^{233}Pa daughter.[105] The isotopic distribution of the Pu stock solution was determined by stippling 1 μL of the 0.5 M HCl stock onto a platinum disc, followed by sequential electrodeposition via induction heating and evaluation by α-spectroscopy on a Tennelec TC 257 spectrometer controlled using ORTEC MAESTRO-32 software. Quantification was performed using InterSpec v1.0.9 (National Technology and Engineering Solutions of Sandia, LLC.).[104] Liquid scintillation counting (LSC) was performed using a Wallac 1414 Guardian liquid scintillation counter controlled with WinSpectral software (PerkinElmer, Inc.). Samples were prepared by diluting 1 μL of metal stock solution in 2 M HCl into 5 mL of Ultima Gold liquid scintillation cocktail (PerkinElmer, Inc.) and mixed by shaking for 5 s. Samples were counted for 10 min with α/β discrimination using the Pulse Shape Analysis function as implemented in WinSpectral.

All investigations of morphology and composition including collection of images and spectra were conducted on a single transmission electron microscope, operated at 200 keV. The samples were prepared by suspending **2-Np** or **2-Pu** in hexane and dropcasting onto the TEM grids. All experimental results were confirmed using several measurements. The microscope used in this study was the FEI TitanX 60−300 microscope at the National Center for Electron Microscopy (NCEM) at LBNL. Images were acquired with a Gatan UltraScan 1000 camera and high-angle annular dark-field detector (HAADF) for scanning transmission electron microscopy (STEM). The FEI TitanX is also equipped with a Bruker SuperX EDS detector, which was used to collect all energy dispersive spectra (EDS). A 1000 series single point Hummingbird Scientific tomography holder was used to hold the specimen. Samples were mounted on 3 mm 300 mesh gold Ultrathin Carbon Film on Lacey Carbon Support Film by Ted Pella, Inc.

Thermal decompositions of homoleptic amidate complexes **1-Np** and **1-Pu** were performed inside an N_2-filled MBraun negative-pressure glovebox by transferring crystalline material to an oven-dried quartz tube, which was then placed upright (nestled in oven-dried ceramic fiber tape) in an oven-dried Al_2O_3 crucible, covered with a crucible lid, and placed inside an MTI 1100C Compact Muffle Furnace (inside the negative pressure glovebox). See Figure 1 for diagram.

Synthesis and Characterization. The preparations of chemically pure stock solutions of ^{237}Np and ^{242}Pu followed procedures adapted from previous reports,[51,52] the full details of which can be accessed in the Supporting Information.

^{237}Np Stock Solution. Residues from past synthetic campaigns were aggregated in 16 M HNO_3 in a 50 mL borosilicate centrifuge tube in a negative-pressure air-filled glovebox. The solution was brought to residue by heating (95 °C), and the fumes were scrubbed by fitting the borosilicate tube with a PTFE stopper featuring an inlet tube fed by an aquarium pump and an outlet tube fed into a Nalgene bottle containing a slurry of $Mg(OH)_2$ in water. The residue was redissolved in 16 M HNO_3 and the procedure was repeated for a total of three cycles. The final residue was dissolved in 2 M HCl and transferred to a 50 mL polypropylene centrifuge tube. The oxidation state was adjusted to $Np^{III/IV}$ (qualitatively assessed by the color change from forest green to deep blue/purple, Figure S21) via the addition of stoichiometric sodium hydroxymethylsulfinate (Rongalite), followed by heating the capped centrifuge tube to 65 °C in an aluminum heating block. After cooling to ambient temperature, 28 M HF was added to the 2 M HCl until the precipitation of a purple/green solid. Note: the presence of green likely indicates incomplete reduction to Np^{III}; however, the supernatant did not contain significant activity by LSC indicating efficient precipitation of the actinides, thus the mixed valent material was carried forward to the next step. The solid was allowed to settle for 4−6 days, then isolated as a pellet by decanting the supernatant and centrifuging the purple/green solid slurry. After washing the NpF_3/NpF_4 pellet (3 × 1 mL H_2O), the solid was transferred as a slurry to a 50 mL polypropylene centrifuge tube and dissolved in a 1:1 mixture of saturated H_3BO_3 and 12 M HCl (alternating 1 mL amounts added until full dissolution of the solid) while heating in an aluminum block at 80 °C). After cooling to ambient temperature, NH_4OH (14.5 M) was added to the solution in equal volume to the 1:1 mixture of H_3BO_3/12 M HCl or until the precipitation of a green solid ($Np(OH)_x(H_2O)_x$) to achieve separation from BF_4^-. The supernatant was evaluated by LSC to ensure efficient precipitation of the actinides, and the solid was isolated as a pellet analogously to the NpF_3/NpF_4. The green $Np(OH)_x(H_2O)_x$ pellet was transferred as a slurry to a 50 mL polypropylene centrifuge tube in secondary containment and dissolved in minimal 9 M HCl before oxidation state adjustment via slow addition of saturated $NaNO_2$ (volume equal to 10% of the 9 M HCl volume). Caution: this step was performed in a tube with at least five times the volume of the ^{237}Np solution and in secondary containment due to the vigorous bubbling and evolution of NO_x fumes even at low concentrations of Np. Once the bubbling and evolution of NO_x fumes had ceased, the oxidation state was confirmed to be Np^{IV} by spiking 10 μL of 9 M HCl solution into 690 μL of 1 M HCl and evaluating by UV−vis−NIR spectroscopy (Figure S2, λ = 724 nm, $\varepsilon \sim 60$; λ = 960 nm, ε = 110).[53,106]

A BioRad column was charged with AG MP-1 anion resin (chloride form, 50−100 mesh, 18 mL for 70 mg ^{237}Np) then preconditioned with Milli-Q H_2O (9 bed volumes) and 12 M HCl (9 bed volumes). The 12 M HCl Np solution was added dropwise to the resin and washed with 12 M HCl (9 bed volumes). The Np was eluted as a well-defined green band upon the addition of 0.5 M HCl (1 bed volume) and collected in the minimal possible volume. A small

https://doi.org/10.1021/acs.inorgchem.4c02099
Inorg. Chem. 2024, 63, 18417−18428

amount (~0.5 mL) of 12 M HCl was spiked into the 0.5 M HCl fraction to stabilize the Np^{IV} oxidation state. Finally, the resin was rinsed with Milli-Q H_2O (9 bed volumes) to elute any remaining ^{233}Pa. The fractions were analyzed by LSC to determine concentration, followed by α-spectroscopy and HPGe to determine isotopic purity. The 0.5 M HCl fraction was passed through a BioRad column charged with prefilter resin (100−150 μm mesh, part no. PF-B200-A, preconditioned with 9 bed volumes Milli-Q H_2O and 9 bed volumes 4 M HCl) to remove residual organics or decomposed resin, and the final concentration of the stock solution determined by LSC.

^{242}Pu Stock Solution. Residues from past synthetic campaigns were purified via sequential dissolution in HNO_3 as described for ^{237}Np. After dissolving the final residue in 6 M HCl and transferring to a polypropylene centrifuge tube, the oxidation state of the Pu was adjusted to $Pu^{III/IV}$ (assessed qualitatively by color change from green to yellow, Figure S22) by addition of excess aqueous NH_2OH HCl and followed by heating (65 °C) while capped. After cooling to ambient temperature, 28 M HF was added to the solution until the precipitation of a red/purple solid. The putative $PuF_3/PuF_4(H_2O)_x$ solid was isolated, washed, and dissolved in H_3BO_3/12 M HCl as described above before the addition of 14.5 M NH_4OH in equal volume to the H_3BO_3/12 M HCl. The tan/green $Pu(OH)_x(H_2O)_x$ solid (green likely due to the presence of $PuO_2(OH)_x$) was isolated and washed as described for ^{237}Np followed by dissolution in 12 M HCl to yield a bright red/orange solution.

A BioRad column was charged with AG MP-1 anion resin (chloride form, 50−100 mesh, 15 mL for 40 mg ^{242}Pu) then preconditioned with Milli-Q H_2O (9 bed volumes) and 12 M HCl (9 bed volumes). The 12 M HCl Pu solution was added dropwise to the resin and washed with 12 M HCl (9 bed volumes). The ^{241}Am (daughter of ^{241}Pu) and Pu were eluted sequentially upon the addition of 4 M HCl, switching receiving cones when the eluent changes color from yellow (^{241}Am, yellow appearance likely due to microgram quantities of ^{242}Pu identified in this fraction by LSC) to light red (^{242}Pu). This was found to be a more efficient separation compared with the reported conditions of eluting with 0.5 M HCl, which we hypothesize is due to the peculiarity of the LBNL ^{242}Pu legacy stock containing ^{241}Pu, which necessitated modified elution conditions. Finally, the resin was rinsed with Milli-Q H_2O (9 bed volumes). The fractions were analyzed by LSC to determine the concentration, followed by α-spectroscopy and HPGe to determine isotopic purity and composition. The 4 M HCl Pu fraction was passed through a BioRad column charged with prefilter resin (100−150 μm particle size, part no. PF-B200-A, preconditioned with 9 bed volumes Milli-Q H_2O and 9 bed volumes 4 M HCl) to remove residual organics or decomposed resin, and the final concentration of the stock solution determined by LSC.

$NpCl_4(DME)_2$. Prepared by adapting from reported procedures,[61,62] the full details of which can be accessed in the Supporting Information: 0.073 g, 0.13 mmol, 86% yield.

$PuCl_4(DME)_2$. Prepared by adapting from reported procedures,[61,62] the full details of which can be accessed in the Supporting Information: 0.033 g, 0.059 mmol, 78% yield.

1-Np ($Np(ITA)_4$). In a negative-pressure N_2-filled glovebox, a 20 mL scintillation vial was charged with $NpCl_4(DME)_2$ (2.43 mL of a 25 mM stock solution of $NpCl_4(DME)_2$ in DME, 60.8 μmol, 1 equiv), capped, and placed in a −35 °C freezer for 10 min. Simultaneously, a separate 20 mL scintillation vial was sequentially charged with an oven-dried stir bar, then K(ITA) (8.30 mL of a 30 mM stock solution of K(ITA) in DME, 249 μmol, 4.1 equiv) and placed in a −35 °C freezer for 10 min. The precooled solution of $NpCl_4(DME)_2$ was added dropwise to the stirring, precooled solution of K(ITA), resulting in a color change to very faint pink-yellow which persisted for the duration of the reaction. The vial was capped and stirred after warming to ambient temperature for 17 h. The reaction was stopped by removing the DME under reduced pressure, resulting in a ballet-pink (Figure S23d) residue mixed with a colorless residue (presumably KCl). The product was extracted into Et_2O and centrifuged in 6 × 1 mL aliquots to remove KCl. The aliquots were combined in a new 20 mL scintillation vial and brought to residue under reduced pressure. The ballet-pink residue was dissolved in minimal Et_2O and placed in a −35 °C freezer to crystallize for 20 h. The product (0.036 g, 44.7 μmol, 73% yield) was isolated as a crop of deep rose-pink, diffraction-quality crystals (Figure S23e, blocks) by removal of the supernatant by decanting, then washed in bulk with *n*-hexane (3 × 1 mL) and dried under reduced pressure before further use. ^1H NMR (tol-d_8, 300 MHz): δ 3.15 (fwhm = 3.39 Hz, 4H, $CH(CH_3)_2$), δ 1.74 (fwhm = 18.47 Hz, 24H, $CH(CH_3)_2$), δ −0.45 (fwhm = 25.11, 36H, $C(CH_3)_3$). UV−vis−NIR (Et_2O): λ_{max} (nm) 413.3, 438.2, 471.4, 490.6, 513.6, 526.3, 547.4, 618.3, 648.4, 662.4, 725.7, 749.9, 788.3, 818.9, 854.7, 873.9, 907.8, 946.1, 970.3, 1006.8, 1175.4, 1192.1.

1-Pu ($Pu(ITA)_4$). In a negative-pressure N_2-filled glovebox, a 20 mL scintillation vial was charged with $PuCl_4(DME)_2$ (536 μL of a 25 mM stock solution of $PuCl_4(DME)_2$ in DME, 13.4 μmol, 1 equiv), capped, and placed in a −35 °C freezer for 10 min. Simultaneously, a separate 20 mL scintillation vial was sequentially charged with an oven-dried stir bar, then K(ITA) (1.80 mL of a 30 mM stock solution of K(ITA) in DME, 53.9 μmol, 4.1 equiv) and placed in a −35 °C freezer for 10 min. The precooled solution of $PuCl_4(DME)_2$ was added dropwise to the stirring, precooled solution of K(ITA), resulting in a brief color change to faint apple green, then to a golden-yellow which persisted for the duration of the reaction. The vial was capped and stirred and warmed to ambient temperature for 17 h. The reaction was stopped by removing the DME under reduced pressure, resulting in a golden-orange residue mixed with a colorless residue (presumably KCl). The product was extracted into Et_2O and centrifuged in 4 × 1 mL aliquots to remove KCl. The aliquots were combined in a new 20 mL scintillation vial and brought to residue under reduced pressure. The golden-orange residue was dissolved in minimal Et_2O and placed in a −35 °C freezer to crystallize for 20 h. The product (0.010 g, 12.3 μmol, 92% yield) was isolated as a crop of bright orange, diffraction-quality crystals (Figure S24, plates) by removal of the supernatant by decanting, then washed in bulk with *n*-hexane (3 × 1 mL) and dried under reduced pressure before further use. ^1H NMR (tol-d_8, 300 MHz): δ 6.52 (fwhm = 37.03 Hz, 4H, $CH(CH_3)_2$), δ 1.71 (fwhm = 13.08 Hz, 36H, $C(CH_3)_3$), δ −0.43 (fwhm = 18.69 Hz, 24H, $CH(CH_3)_2$). UV−vis−NIR (Et_2O): λ_{max} (nm) 543.6, 577.4, 666.3, 697.6, 769.8, 796.6, 827.9, 871.3, 1029.8, 1053.4, 1089.8, 1185.0, 1241.9

2a-Np (NpO_2). In a negative-pressure N_2-filled glovebox, **1-Np** (7.0 mg, 9 μmol, pink crystals) was suspended in *n*-hexane and transferred to a preweighed quartz tube (cut to 1.5 in length) in a 20 mL scintillation vial. The crystals were dried via gently blowing N_2 facilitated by an aquarium pump equipped with tubing attached to a 200 μL pipet tip fed through a septum. The quartz tube was transferred to a crucible charged with a spiral of ceramic fiber tape to ensure uniform heating and so that the sample remains stable and upright for the duration of the thermolysis (see Figure 1d for diagram). The crucible was capped with a matching lid and placed inside an MTI 1100C Compact Muffle Furnace modified with an inlet and outlet hole in the back. The sample was thermolyzed at 270 °C following the ramping program in Table S2. After cooling to ambient temperature, the sample was removed from the furnace and the product isolated as a fluffy mustard-yellow powder (Figure S25, 2.6 mg, quantitative yield) suitable for analysis by electron microscopy (EM).

2a-Pu (PuO_2). Prepared identically to **2a-Np**, and isolated as a fluffy olive-green powder (Figure S26, 1.0 mg, 84% yield) suitable for analysis by EM.

2b-Np (NpO_2). Prepared identically to **2a-Np**, with an additional annealing step: the sample was thermolyzed at 270 °C and annealed at 850 °C following the ramping program in Table S3. After cooling to ambient temperature, the sample was removed from the furnace and the product isolated as a deep olive-green microcrystalline powder (Figure S27, 6.0 mg, 97% yield) suitable for analysis by powder X-ray diffraction.

2b-Pu (PuO_2). Prepared identically to **2b-Np**, and isolated as a black microcrystalline powder (Figure S28, 1.2 mg, 93% yield) suitable for analysis by powder X-ray diffraction.

https://doi.org/10.1021/acs.inorgchem.4c02099
Inorg. Chem. 2024, 63, 18417−18428

■ ASSOCIATED CONTENT

Supporting Information

The Supporting Information is available free of charge at https://pubs.acs.org/doi/10.1021/acs.inorgchem.4c02099.

Materials, methods, and general considerations; synthesis and characterization; photographs of synthetic procedures and sample preparation; X-ray crystallographic data; NMR spectra; UV−vis spectra (PDF)

Accession Codes

CCDC 2371362−2371363 contain the supplementary crystallographic data for this paper. These data can be obtained free of charge via www.ccdc.cam.ac.uk/data_request/cif., or by emailing data_request@ccdc.cam.ac.uk, or by contacting The Cambridge Crystallographic Data Centre, 12 Union Road, Cambridge CB2 1EZ, UK; fax: +44 1223 336 033.

■ AUTHOR INFORMATION

Corresponding Authors

John Arnold − *Chemical Sciences Division, Lawrence Berkeley National Laboratory, Berkeley, California 94720, United States; Department of Chemistry, University of California, Berkeley, Berkeley, California 94720, United States;* orcid.org/0000-0001-9671-227X; Email: arnold@berkeley.edu

Rebecca J. Abergel − *Chemical Sciences Division, Lawrence Berkeley National Laboratory, Berkeley, California 94720, United States; Department of Chemistry and Department of Nuclear Engineering, University of California, Berkeley, Berkeley, California 94720, United States;* orcid.org/0000-0002-3906-8761; Email: rjabergel@lbl.gov

Stefan G. Minasian − *Chemical Sciences Division, Lawrence Berkeley National Laboratory, Berkeley, California 94720, United States;* orcid.org/0000-0003-1346-7497; Email: sgminasian@lbl.gov

Authors

Appie Peterson − *Chemical Sciences Division, Lawrence Berkeley National Laboratory, Berkeley, California 94720, United States*

Sheridon N. Kelly − *Chemical Sciences Division, Lawrence Berkeley National Laboratory, Berkeley, California 94720, United States; Department of Chemistry, University of California, Berkeley, Berkeley, California 94720, United States*

Trevor Arino − *Chemical Sciences Division, Lawrence Berkeley National Laboratory, Berkeley, California 94720, United States; Department of Nuclear Engineering, University of California, Berkeley, Berkeley, California 94720, United States*

S. Olivia Gunther − *Chemical Sciences Division, Lawrence Berkeley National Laboratory, Berkeley, California 94720, United States*

Erik T. Ouellette − *Chemical Sciences Division, Lawrence Berkeley National Laboratory, Berkeley, California 94720, United States; Department of Chemistry, University of California, Berkeley, Berkeley, California 94720, United States;* orcid.org/0000-0003-2138-6259

Jennifer N. Wacker − *Chemical Sciences Division, Lawrence Berkeley National Laboratory, Berkeley, California 94720, United States*

Joshua J. Woods − *Chemical Sciences Division, Lawrence Berkeley National Laboratory, Berkeley, California 94720, United States;* orcid.org/0000-0002-6213-4093

Simon J. Teat − *Advanced Light Source, Lawrence Berkeley National Laboratory, Berkeley, California 94720, United States*

Wayne W. Lukens − *Chemical Sciences Division, Lawrence Berkeley National Laboratory, Berkeley, California 94720, United States;* orcid.org/0000-0002-0796-7631

Complete contact information is available at: https://pubs.acs.org/10.1021/acs.inorgchem.4c02099

Author Contributions

A.P., S.N.K., and S.O.G. performed the syntheses and collected characterization data, A.P. analyzed the data. A.P., E.T.O., S.N.K., and J.N.W. collected SCXRD data, S.J.T. solved the X-ray structures and manages the small-molecule crystallography beamline (12.2.1) at the ALS. T.A. collected and analyzed STEM and EDS data, A.P. and S.O.G. prepared the samples. J.N.W. designed the PXRD experiments. A.P. and W.W.L. designed the experimental procedures, and J.J.W. supported the transuranic chemistry engineering controls and protocols. A.P. wrote the manuscript and Supporting Information, with editorial contributions from all authors.

Notes

The authors declare no competing financial interest.

■ ACKNOWLEDGMENTS

The work described here was supported by the U.S. Department of Energy (DOE), Office of Science, Office of Basic Energy Sciences, Chemical Sciences, Geosciences, and Biosciences Division, Heavy Element Chemistry Program at LBNL under contract DE-AC02-05CH11231. AP was supported by the DOE's National Nuclear Security Administration's Office of Defense Nuclear Nonproliferation Research and Development (NA-22) as part of the NextGen Nonproliferation Leadership Development Program. S.N.K. was supported by a DOE Integrated University Program Fellowship at the University of California, Berkeley. This research used resources of the Advanced Light Source, which is a DOE Office of Science User Facility under contract no. DE-AC02-05CH11231. We thank Dr. Karen C. Bustillo for assistance in our studies at the Molecular Foundry, which is supported by the DOE, Office of Science, Office of Basic Energy Sciences, under contract no. DE-AC02-05CH11231.

■ REFERENCES

(1) Guaita, N. *Uncovering Hidden Market Opportunities for Advanced Nuclear Reactors*, INL/MIS-23−74499-Rev000; Idaho National Laboratory (INL): Idaho Falls, ID, United States, 2023.

(2) Hoffman, D. C. Exploring the Frontiers of Nuclear and Radiochemistry. *J. Nucl. Radiochem. Sci* **2007**, *8* (2), 35−38.

(3) Carter, K. P.; Pallares, R. M.; Abergel, R. J. Open Questions in Transplutonium Coordination Chemistry. *Commun. Chem* **2020**, *3* (1), 103.

(4) McDonald, L. W.; Sentz, K.; Hagen, A.; Chung, B. W.; Nizinski, C. A.; Schwerdt, I. J.; Hanson, A.; Donald, S.; Clark, R.; Sjoden, G.; et al. Review of Multi-Faceted Morphologic Signatures of Actinide Process Materials for Nuclear Forensic Science. *J. Nucl. Mater* **2024**, *588*, 154779.

(5) Straub, M. D.; Arnold, J.; Fessenden, J.; Kiplinger, J. L. Recent Advances in Nuclear Forensic Chemistry. *Anal. Chem* **2021**, *93* (1), 3−22.

(6) Batuk, O. N.; Conradson, S. D.; Aleksandrova, O. N.; Boukhalfa, H.; Burakov, B. E.; Clark, D. L.; Czerwinski, K. R.; Felmy, A. R.; Lezama-Pacheco, J. S.; Kalmykov, S. N.; et al. Multiscale Speciation of U and Pu at Chernobyl, Hanford, Los Alamos, McGuire AFB, Mayak, and Rocky Flats. *Environ. Sci. Technol* **2015**, *49* (11), 6474−6484.
(7) Clark, D. L.; Janecky, D. R.; Lane, L. J. Science-Based Cleanup of Rocky Flats. *Phys. Today* **2006**, *59* (9), 34−40.
(8) Walther, C.; Denecke, M. A. Actinide Colloids and Particles of Environmental Concern. *Chem. Rev* **2013**, *113* (2), 995−1015.
(9) Romanchuk, A. Y.; Kalmykov, S. N.; Kersting, A. B.; Zavarin, M. Behavior of Plutonium in the Environment. *Russ. Chem. Rev* **2016**, *85* (9), 995−1010.
(10) Moore, K. T. X-Ray and Electron Microscopy of Actinide Materials. *Micron* **2010**, *41* (4), 336−358.
(11) Moore, K. T.; van der Laan, G. Accurate Labeling of the Light-Actinide O4,5 Edges. *Ultramicroscopy* **2007**, *107* (12), 1201−1206.
(12) Neidig, M. L.; Clark, D. L.; Martin, R. L. Covalency in F-Element Complexes. *Coord. Chem. Rev* **2013**, *257* (2), 394−406.
(13) Modin, A.; Suzuki, M.-T.; Vegelius, J.; Yun, Y.; Shuh, D. K.; Werme, L.; Nordgren, J.; Oppeneer, P. M.; Butorin, S. M. 5 *f* -Shell Correlation Effects in Dioxides of Light Actinides Studied by O 1*s* X-Ray Absorption and Emission Spectroscopies and First-Principles Calculations. *J. Phys.: condens. Matter* **2015**, *27* (31), 315503.
(14) Buck, E.; Sinkov, S.; Reilly, D.; Lach, T.; Ilton, E. *Scanning Transmission Electron Microscopy of Plutonium Particles in Hanford Tanks 241-TX-118 and 241-SY-102* **2019**, PNNL−29553.
(15) Vallejo, K. D.; Kabir, F.; Poudel, N.; Marianetti, C. A.; Hurley, D. H.; Simmonds, P. J.; Dennett, C. A.; Gofryk, K. Advances in Actinide Thin Films: Synthesis, Properties, and Future Directions. *Rep. Prog. Phys* **2022**, *85* (12), 123101.
(16) Wen, X.-D.; Loble, M. W.; Batista, E. R.; Bauer, E.; Boland, K. S.; Burrell, A. K.; Conradson, S. D.; Daly, S. R.; Kozimor, S. A.; Minasian, S. G.; Martin, R. L.; McCleskey, T. M.; Scott, B. L.; Shuh, D. K.; Tyliszczak, T. Electronic Structure and O K-Edge XAS Spectroscopy of U_3O_8. *J. Electron Spectrosc. Relat. Phenom* **2014**, *194*, 81−87.
(17) Colle, J.-Y.; Naji, M.; Sierig, M.; Manara, D. A Novel Technique for Raman Analysis of Highly Radioactive Samples Using Any Standard Micro-Raman Spectrometer. *J. Vis. Exp.* **2017**, No. 122, No. e54889.
(18) Corbey, J. F.; Sweet, L. E.; Sinkov, S. I.; Reilly, D. D.; Parker, C. M.; Lonergan, J. M.; Johnson, T. J. Quantitative Microstructural Characterization of Plutonium Oxalate Auto-Degradation and Evidence for PuO_2 Nanocrystal Formation. *Eur. J. Inorg. Chem* **2021**, *2021* (32), 3277−3291.
(19) Enriquez, E.; Wang, G.; Sharma, Y.; Sarpkaya, I.; Wang, Q.; Chen, D.; Winner, N.; Guo, X.; Dunwoody, J.; White, J.; et al. Structural and Optical Properties of Phase-Pure UO_2, α-U_3O_8, and α-UO_3 Epitaxial Thin Films Grown by Pulsed Laser Deposition. *ACS Appl. Mater. Interfaces* **2020**, *12* (31), 35232−35241.
(20) Conradson, S. D.; Begg, B. D.; Clark, D. L.; Den Auwer, C.; Espinosa-Faller, F. J.; Gordon, P. L.; Hess, N. J.; Hess, R.; Keogh, D. W.; Morales, L. A.; et al. Speciation and Unusual Reactivity in PuO_{2+x}. *Inorg. Chem* **2003**, *42* (12), 3715−3717.
(21) De Bruycker, F.; Boboridis, K.; Pöml, P.; Eloirdi, R.; Konings, R. J. M.; Manara, D. The Melting Behaviour of Plutonium Dioxide: A Laser-Heating Study. *J. Nucl. Mater.* **2011**, *416* (1), 166−172.
(22) Sarsfield, M. J.; Taylor, R. J.; Puxley, C.; Steele, H. M. Raman Spectroscopy of Plutonium Dioxide and Related Materials. *J. Nucl. Mater.* **2012**, *427* (1), 333−342.
(23) Vigier, N.; Grandjean, S.; Arab-Chapelet, B.; Abraham, F. Reaction Mechanisms of the Thermal Conversion of Pu(IV) Oxalate into Plutonium Oxide. *J. Alloys Compd.* **2007**, *444*−*445*, 594−597.
(24) Peruski, K. M.; Powell, B. A. Effect of Calcination Temperature on Neptunium Dioxide Microstructure and Dissolution. *Environ. Sci.: Nano* **2020**, *7*, 3869.
(25) Conradson, S. D.; Begg, B. D.; Clark, D. L.; den Auwer, C.; Ding, M.; Dorhout, P. K.; Espinosa-Faller, F. J.; Gordon, P. L.; Haire, R. G.; Hess, N. J.; et al. Local and Nanoscale Structure and Speciation in the $PuO_{2+x-y}(OH)_{2y}{\cdot}zH_2O$ System. *J. Am. Chem. Soc* **2004**, *126* (41), 13443−13458.
(26) Ao, B.; Qiu, R.; Lu, H.; Ye, X.; Shi, P.; Chen, P.; Wang, X. New Insights into the Formation of Hyperstoichiometric Plutonium Oxides. *J. Phys. Chem. C* **2015**, *119* (1), 101−108.
(27) Haschke, J. M.; Allen, T. H.; Morales, L. A. Reaction of Plutonium Dioxide with Water: Formation and Properties of PuO_{2+x}. *Science* **2000**, *287* (5451), 285−287.
(28) Neilson, W. D.; Pegg, J. T.; Steele, H.; Murphy, S. T. The Defect Chemistry of Non-Stoichiometric $PuO_{2\pm x}$. *Phys. Chem. Chem. Phys.* **2021**, *23* (8), 4544−4554.
(29) Morss, L. R.; Edelstein, N.; Fuger, J.; Katz, J. J. *Chemistry of Actinide and Transactinide Elements - Fourth Edition*; Springer, 2010.
(30) Machuron-Mandard, X.; Madic, C. Plutonium Dioxide Particle Properties as a Function of Calcination Temperature. *J. Alloys Compd.* **1996**, *235* (2), 216−224.
(31) *Actinide Nanoparticle Research*; Kalmykov, S. N.; Denecke, M. A., Eds.; Springer: Berlin, Heidelberg, 2011.
(32) Caciuffo, R.; Lander, G. H.; van der Laan, G. Synchrotron Radiation Techniques and Their Application to Actinide Materials. *Rev. Mod. Phys.* **2023**, *95* (1), 015001.
(33) Runde, W.; Brodnax, L. F.; Goff, G.; Bean, A. C.; Scott, B. L. Directed Synthesis of Crystalline Plutonium(III) and (IV) Oxalates: Accessing Redox-Controlled Separations in Acidic Solutions. *Inorg. Chem.* **2009**, *48* (13), 5967−5972.
(34) Hainje, C. M.; Nizinski, C. A.; Jackson, S. W.; Clark, R. A.; Heller, F. D.; Schwerdt, I. J.; Buck, E. C.; Meier, D. E.; Hagen, A. R. Investigation of Process History and Underlying Phenomena Associated with the Synthesis of Plutonium Oxides Using Vector Quantizing Variational Autoencoder. *Chemom. Intell. Lab. Syst.* **2023**, *240*, 104909.
(35) Andreev, G.; Budantseva, N.; Fedoseev, A.; Moisy, P. Polymeric Structure of Oxalato-Bridged Complexes of Tetravalent Actinides Th, U, Np and Pu. *Inorg. Chem.* **2011**, *50* (22), 11481−11486.
(36) Scott, B. L.; Pugmire, A. L.; Stritzinger, J. T.; Veirs, D. K.; Wolfsberg, L. E.; Wilkerson, M. P. Relationships between Experimental Signatures and Processing History for a Variety of PuO_2 Materials. *J. Nucl. Mater.* **2019**, *521*, 155−160.
(37) Virot, M.; Dumas, T.; Cot-Auriol, M.; Moisy, P.; Nikitenko, S. I. Synthesis and Multi-Scale Properties of PuO_2 Nanoparticles: Recent Advances and Open Questions. *Nanoscale Adv.* **2022**, *4* (23), 4938−4971.
(38) Villa-Aleman, E.; Dick, D. D.; Christian, J. H.; Foley, B. J.; Roy, L. E. The Electronic Raman Scattering Spectrum of PuO2. *J. Raman Spectrosc.* **2023**, *54* (3), 324−332.
(39) Tamain, C.; Arab-Chapelet, B.; Rivenet, M.; Legoff, X. F.; Loubert, G.; Grandjean, S.; Abraham, F. Coordination Modes of Americium in the $Am_2(C_2O_4)_3(H_2O)_6{\cdot}4H_2O$ Oxalate: Synthesis, Crystal Structure, Spectroscopic Characterizations and Comparison in the $M_2(C_2O_4)_3(H_2O)_6{\cdot}nH_2O$ (M = Ln, An) Series. *Inorg. Chem.* **2016**, *55* (1), 51−61.
(40) Springell, R.; Lawrence Bright, E.; Chaney, D. A.; Harding, L. M.; Bell, C.; Ward, R. C. C.; Lander, G. H. A Review of Uranium-Based Thin Films. *Adv. Phys.* **2022**, *71* (3−4), 87−165.
(41) Han, X.; Alcock, N. M.; Kaltsoyannis, N. Effect of Point Defects on Water Adsorption on the ThO2{111} Surface: A First-Principles Computational Study. *J. Nucl. Mater.* **2024**, *588*, 154763.
(42) Chen, J.-L.; Kaltsoyannis, N. Hybrid Functional/Embedded Cluster Study of Uranium and Actinide (Actinide = Np, Pu, Am or Cm) Mixed Dioxides Bulk and {110} Surfaces. *J. Nucl. Mater.* **2022**, *560*, 153490.
(43) Han, X.; Kaltsoyannis, N. Reactions of NO and H_2O on the PuO_2 {111} Surface: A DFT Study. *J. Nucl. Mater.* **2023**, *575*, 154240.
(44) Scott, B. L.; Joyce, J. J.; Durakiewicz, T. D.; Martin, R. L.; McCleskey, T. M.; Bauer, E.; Luo, H.; Jia, Q. High Quality Epitaxial Thin Films of Actinide Oxides, Carbides, and Nitrides: Advancing Understanding of Electronic Structure of f-Element Materials. *Coord. Chem. Rev.* **2014**, *266*−*267*, 137−154.

https://doi.org/10.1021/acs.inorgchem.4c02099
Inorg. Chem. 2024, 63, 18417−18428

(45) Mark McCleskey, T.; Bauer, E.; Jia, Q.; Burrell, A. K.; Scott, B. L.; Conradson, S. D.; Mueller, A.; Roy, L.; Wen, X.; Scuseria, G. E.; et al. Optical Band Gap of NpO_2 and PuO_2 from Optical Absorbance of Epitaxial Films. *J. Appl. Phys.* **2013**, *113* (1), 013515.
(46) Edelmann, F. T. Lanthanide Amidinates and Guanidinates in Catalysis and Materials Science: A Continuing Success Story. *Chem. Soc. Rev.* **2012**, *41* (23), 7657−7672.
(47) Thiede, T. B.; Krasnopolski, M.; Milanov, A. P.; de Los Arcos, T.; Ney, A.; Becker, H.-W.; Rogalla, D.; Winter, J.; Devi, A.; Fischer, R. A. Evaluation of Homoleptic Guanidinate and Amidinate Complexes of Gadolinium and Dysprosium for MOCVD of Rare-Earth Nitride Thin Films. *Chem. Mater.* **2011**, *23* (6), 1430−1440.
(48) Appel, L.; Leduc, J.; Webster, C. L.; Ziller, J. W.; Evans, W. J.; Mathur, S. Synthesis of Air-Stable, Volatile Uranium(IV) and (VI) Compounds and Their Gas-Phase Conversion To Uranium Oxide Films. *Angew. Chem., Int. Ed.* **2015**, *54* (7), 2209−2213.
(49) Straub, M. D.; Leduc, J.; Frank, M.; Raauf, A.; Lohrey, T. D.; Minasian, S. G.; Mathur, S.; Arnold, J. Chemical Vapor Deposition of Phase-Pure Uranium Dioxide Thin Films from Uranium(IV) Amidate Precursors. *Angew. Chem., Int. Ed.* **2019**, *58* (17), 5749−5753.
(50) Straub, M. D.; Ouellette, E. T.; Boreen, M. A.; Branson, J. A.; Ditter, A.; Kilcoyne, A. L. D.; Lohrey, T. D.; Marcus, M. A.; Paley, M.; Ramirez, J.; et al. Thorium Amidates Function as Single-Source Molecular Precursors for Thorium Dioxide. *Chem. Commun.* **2021**, *57* (40), 4954−4957.
(51) Mounce, A. M.; Yasuoka, H.; Koutroulakis, G.; Lee, J. A.; Cho, H.; Gendron, F.; Zurek, E.; Scott, B. L.; Trujillo, J. A.; Slemmons, A. K.; et al. Nuclear Magnetic Resonance Measurements and Electronic Structure of Pu(IV) in $[(Me)_4N]_2PuCl_6$. *Inorg. Chem.* **2016**, *55* (17), 8371−8380.
(52) Cary, S. K.; Livshits, M.; Cross, J. N.; Ferrier, M. G.; Mocko, V.; Stein, B. W.; Kozimor, S. A.; Scott, B. L.; Rack, J. J. Advancing Understanding of the + 4 Metal Extractant Thenoyltrifluoroacetonate (TTA^-); Synthesis and Structure of $M^{IV}TTA_4$ (M^{IV} = Zr, Hf, Ce, Th, U, Np, Pu) and $M^{III}(TTA)_4^-$ (M^{III} = Ce, Nd, Sm, Yb). *Inorg. Chem.* **2018**, *57* (7), 3782−3797.
(53) Burney, G. A.; Harbour, R. M. *Radiochemistry of Neptunium*; The National Academies Press, 1974.
(54) Li, C.; Thomson, R. K.; Gillon, B.; Patrick, B. O.; Schafer, L. L. Amidate Complexes of Titanium and Zirconium: A New Class of Tunable Precatalysts for the Hydroamination of Alkynes. *Chem. Commun.* **2003**, No. 19, 2462.
(55) Catherall, A. L.; Hill, M. S.; Johnson, A. L.; Kociok-Köhn, G.; Mahon, M. F. Homoleptic Zirconium Amidates: Single Source Precursors for the Aerosol-Assisted Chemical Vapour Deposition of ZrO_2. *J. Mater. Chem. C* **2016**, *4* (45), 10731−10739.
(56) Straub, M. D.; Ouellette, E. T.; Boreen, M. A.; Britt, R. D.; Chakarawet, K.; Douair, I.; Gould, C. A.; Maron, L.; Del Rosal, I.; Villarreal, D.; et al. A Uranium(II) Arene Complex That Acts as a Uranium(I) Synthon. *J. Am. Chem. Soc* **2021**, *143* (47), 19748−19760.
(57) Straub, M. D.; Hohloch, S.; Minasian, S. G.; Arnold, J. Homoleptic U(III) and U(IV) amidate complexes. *Dalton Trans* **2018**, *47* (6), 1772−1776.
(58) Ma, C.-G.; Brik, M. G.; Liu, D.-X.; Feng, B.; Tian, Y.; Suchocki, A. Energy Level Schemes of f^N Electronic Configurations for the Di-, Tri-, and Tetravalent Lanthanides and Actinides in a Free State. *J. Lumin.* **2016**, *170*, 369−374.
(59) Schnaars, D. D.; Gaunt, A. J.; Hayton, T. W.; Jones, M. B.; Kirker, I.; Kaltsoyannis, N.; May, I.; Reilly, S. D.; Scott, B. L.; Wu, G. Bonding Trends Traversing the Tetravalent Actinide Series: Synthesis, Structural, and Computational Analysis of $An^{IV}(^{Ar}acnac)_4$ Complexes (An = Th, U, Np, Pu; $^{Ar}acnac$ = $^{Ar}NC(Ph)CHC(Ph)O$; Ar = 3,5-$^tBu_2C_6H_3$). *Inorg. Chem.* **2012**, *51* (15), 8557−8566.
(60) Su, J.; Cheisson, T.; McSkimming, A.; Goodwin, C. A. P.; DiMucci, I. M.; Albrecht-Schönzart, T.; Scott, B. L.; Batista, E. R.; Gaunt, A. J.; Kozimor, S. A.; Yang, P. Complexation and Redox Chemistry of Neptunium, Plutonium and Americium with a Hydroxylaminato Ligand. *Chem. Sci.* **2021**, *12* (40), 13343−13359.
(61) Reilly, S. D.; Brown, J. L.; Scott, B. L.; Gaunt, A. J. Synthesis and Characterization of $NpCl_4(DME)_2$ and $PuCl_4(DME)_2$ Neutral Transuranic An(IV) Starting Materials. *Dalton Trans.* **2014**, *43* (4), 1498−1501.
(62) Goodwin, C. A. P.; Janicke, M. T.; Scott, B. L.; Gaunt, A. J. $[AnI_3(THF)_4]$ (An = Np, Pu) Preparation Bypassing An^0 Metal Precursors: Access to Np^{3+}/Pu^{3+} Nonaqueous and Organometallic Complexes. *J. Am. Chem. Soc.* **2021**, *143* (49), 20680−20696.
(63) Cary, S. K.; Boland, K. S.; Cross, J. N.; Kozimor, S. A.; Scott, B. L. Advances in Containment Methods and Plutonium Recovery Strategies That Led to the Structural Characterization of Plutonium-(IV) Tetrachloride Tris-Diphenylsulfoxide, $PuCl_4(OSPh_2)_3$. *Polyhedron* **2017**, *126*, 220−226.
(64) Budantseva, N. A.; Grigor'ev, M. S.; Mishkevich, V. I.; Sokolova, M. N.; Fedoseev, A. M. *Koord. Khimiia* **2011**, *37*, 703.
(65) Charushnikova, I. A.; Starikova, Z. A.; Shirokova, I. B.; Fedoseev, A. M.; Grigor'ev, M. S.; Budantseva, N. A. *Koord. Khimiia* **2003**, *29*, 290.
(66) Zhang, Z.; Parker, B. F.; Lohrey, T. D.; Teat, S. J.; Arnold, J.; Rao, L. Complexation-Assisted Reduction: Complexes of Glutaroimide-Dioxime with Tetravalent Actinides (Np(IV) and Th(IV)). *Dalton Trans.* **2018**, *47* (24), 8134−8141.
(67) Bagnall, K. W.; Payne, G. F.; Alcock, N. W.; Flanders, D. J.; Brown, D. Actinide Structural Studies. Part 8. Some New Oxygen-Donor Complexes of Trichloro(Cyclopentadienyl)Neptunium(IV); the Crystal Structure of Trichloro(η^5-Cyclopentadienyl)Bis-(Methyldiphenylphosphine Oxide)Neptunium(IV). *J. Chem. Soc., Dalton Trans.* **1986**, No. 4, 783−787.
(68) Radoske, T.; März, J.; Patzschke, M.; Kaden, P.; Walter, O.; Schmidt, M.; Stumpf, T. Bonding Trends in Tetravalent Th−Pu Monosalen Complexes. *Chem. − Eur. J* **2020**, *26* (70), 16853−16859.
(69) Charushnikova, I. A.; Krot, N. N.; Grigor'ev, M. S. Cation-Cation Interaction in Mixed-Valent An(IV)/Np(V) Tribromoacetates $[An(NpO_2)(H_2O)_3(CBr_3COO)_5]\cdot CBr_3COOH\cdot nH_2O$, An = Th(IV), Np(IV). *Radiochemistry* **2014**, *56* (5), 468−475.
(70) Bansal, D.; Kaden, P.; Patzschke, M.; März, J.; Schmidt, M. Comparative Analysis of Mononuclear 1:1 and 2:1 Tetravalent Actinide (U, Th, Np) Complexes: Crystal Structure, Spectroscopy, and Electrochemistry. *Inorg. Chem.* **2022**, *61* (27), 10509−10520.
(71) Kloditz, R.; Radoske, T.; Schmidt, M.; Heine, T.; Stumpf, T.; Patzschke, M. Comprehensive Bonding Analysis of Tetravalent F-Element Complexes of the Type $[M(Salen)_2]$. *Inorg. Chem.* **2021**, *60* (4), 2514−2525.
(72) Zhang, J.; Wenzel, M.; Schnaars, K.; Hennersdorf, F.; Schwedtmann, K.; März, J.; Rossberg, A.; Kaden, P.; Kraus, F.; Stumpf, T.; et al. Coordination of Trivalent Lanthanum and Cerium, and Tetravalent Cerium and Actinides (An = $Th_{(IV)}$, $U_{(IV)}$, $Np_{(IV)}$) by a 4-Phosphoryl 1H-Pyrazol-5-Olate Ligand in Solution and the Solid State. *Dalton Trans.* **2021**, *50* (10), 3550−3558.
(73) Klamm, B. E.; Windorff, C. J.; Celis-Barros, C.; Beltran-Leiva, M. J.; Sperling, J. M.; Albrecht-Schönzart, T. E. Exploring the Oxidation States of Neptunium with Schiff Base Coordination Complexes. *Inorg. Chem.* **2020**, *59* (24), 18035−18047.
(74) Brewster, J. T.; Mangel, D. N.; Gaunt, A. J.; Saunders, D. P.; Zafar, H.; Lynch, V. M.; Boreen, M. A.; Garner, M. E.; Goodwin, C. A. P.; Settineri, N. S.; et al. In-Plane Thorium(IV), Uranium(IV), and Neptunium(IV) Expanded Porphyrin Complexes. *J. Am. Chem. Soc.* **2019**, *141* (44), 17867−17874.
(75) Tamain, C.; Autillo, M.; Guillaumont, D.; Guérin, L.; Wilson, R. E.; Berthon, C. Structural and Bonding Analysis in Monomeric Actinide(IV) Oxalate from Th(IV) to Pu(IV): Comparison with the An(IV) Nitrate Series. *Inorg. Chem.* **2022**, *61* (31), 12337−12348.
(76) Johnson, A. T.; Parker, T. G.; Dickens, S. M.; Pfeiffer, J. K.; Oliver, A. G.; Wall, D.; Wall, N. A.; Finck, M. R.; Carney, K. P. Synthesis and Crystal Structures of Volatile Neptunium(IV) β-Diketonates. *Inorg. Chem.* **2017**, *56* (21), 13553−13561.
(77) Radoske, T.; Kloditz, R.; Fichter, S.; März, J.; Kaden, P.; Patzschke, M.; Schmidt, M.; Stumpf, T.; Walter, O.; Ikeda-Ohno, A. Systematic Comparison of the Structure of Homoleptic Tetradentate

https://doi.org/10.1021/acs.inorgchem.4c02099
Inorg. Chem. 2024, 63, 18417−18428

N_2O_2-Type Schiff Base Complexes of Tetravalent f-Elements (M(IV) = Ce, Th, U, Np, and Pu) in Solid State and in Solution. *Dalton Trans.* **2020**, *49* (48), 17559−17570.
(78) Allard, B.; Dhabanandana, S.; Krogh-Moe, J.; Songstad, J.; Pilotti, Å. The Crystal Structure of *β*-Tetrakis (acetylacetonato)-neptunium(IV). *Acta Chem. Scand.* **1972**, *26* (9), 3492−3504.
(79) Köhler, L.; Patzschke, M.; Schmidt, M.; Stumpf, T.; März, J. How 5 f Electron Polarisability Drives Covalency and Selectivity in Actinide N-Donor Complexes. *Chem. − Eur. J.* **2021**, *27* (72), 18058−18065.
(80) Matonic, J. H.; Enriquez, A. E.; Scott, B. L.; Paine, R. T.; Neu, M. P. E. Eight and Nine-Coordinate Plutonium (IV) Complexes of the f-Element Extractant 2,5-Bis(diphenylphosphinomethyl)benzene P,P'-dioxide Including Structural Characterization of a Plutonium (IV) Alkoxide. *J. Nucl. Sci. Technol.* **2002**, *39* (sup3), 400−405.
(81) George, K.; Muller, J.; Berthon, L.; Berthon, C.; Guillaumont, D.; Vitorica-Yrezabal, I. J.; Stafford, H. V.; Natrajan, L. S.; Tamain, C. Exploring the Coordination of Plutonium and Mixed Plutonyl−Uranyl Complexes of Imidodiphosphinates. *Inorg. Chem.* **2019**, *58* (10), 6904−6917.
(82) Grigoriev, M. S.; Krot, N. N.; Bessonov, A. A.; Lyssenko, K. A. Lithium(I) Hexaamminecobalt(III) Tetrakis(Malonato-κ^2O,O″)-Plutonate(IV) Pentahydrate. *Acta Crystallogr., Sect. E: Struct. Rep. Online* **2006**, *62* (11), m2889−m2890.
(83) Surbella, R. G.; Ducati, L. C.; Autschbach, J.; Pellegrini, K. L.; McNamara, B. K.; Schwantes, J. M.; Cahill, C. L. Plutonium Chlorido Nitrato Complexes: Ligand Competition and Computational Metrics for Assembly and Bonding. *Chem. Commun.* **2018**, *54* (85), 12014−12017.
(84) Carter, T. J.; Wilson, R. E. Coordination Chemistry of Homoleptic Actinide(IV)−Thiocyanate Complexes. *Chem. − Eur. J.* **2015**, *21* (44), 15575−15582.
(85) Jones, M. B.; Gaunt, A. J. Recent Developments in Synthesis and Structural Chemistry of Nonaqueous Actinide Complexes. *Chem. Rev.* **2013**, *113* (2), 1137−1198.
(86) Benedict, U.; Dabos, S.; Dufour, C.; Spirlet, J. C.; Pagès, M. Neptunium Compounds under High Pressure. *J. Less Common Met.* **1986**, *121*, 461−468.
(87) Chu, M.; Meng, D.; Xiao, S.; Wang, W.; Chen, Q. Evaluation of Thermal Properties of PuO_2 and α-Pu_2O_3 by Atomic Simulation. *J. Alloys Compd.* **2012**, *539*, 7−11.
(88) Scherrer, P. Nachr Ges Wiss Goettingen. *Math Phys.* **1918**, *2*, 98−100.
(89) Holzwarth, U.; Gibson, N. The Scherrer Equation versus the "Debye-Scherrer Equation". *Nat. Nanotechnol.* **2011**, *6* (9), 534−534.
(90) Hudry, D.; Apostolidis, C.; Walter, O.; Janßen, A.; Manara, D.; Griveau, J.-C.; Colineau, E.; Vitova, T.; Prüßmann, T.; Wang, D.; et al. Ultra-Small Plutonium Oxide Nanocrystals: An Innovative Material in Plutonium Science. *Chem. - Eur. J.* **2014**, *20* (33), 10431−10438.
(91) Frontzek, M. D.; Sadergaski, L. R.; Cary, S. K.; Rai, B. K. Search for Octupolar Order in NpO_2 by Neutron Powder Diffraction. *J. Solid State Chem.* **2023**, *321*, 123875.
(92) Liu, J.-B.; Chen, G. P.; Huang, W.; Clark, D. L.; Eugen Schwarz, W. H.; Li, J. Bonding Trends across the Series of Tricarbonato-Actinyl Anions $[(AnO_2)(CO_3)_3]^{4-}$ (An = U−Cm): The Plutonium Turn. *Dalton Trans.* **2017**, *46* (8), 2542−2550.
(93) Wacker, J. N.; Han, S. Y.; Murray, A. V.; Vanagas, N. A.; Bertke, J. A.; Sperling, J. M.; Surbella, R. G. I.; Knope, K. E. From Thorium to Plutonium: Trends in Actinide(IV) Chloride Structural Chemistry. *Inorg. Chem.* **2019**, *58* (16), 10578−10591.
(94) Autillo, M.; Illy, M.-C.; Briscese, L.; Islam, M. A.; Bolvin, H.; Berthon, C. Paramagnetic Properties of $[An^{IV}(NO_3)_6]^{2-}$ Complexes (An = U, Np, Pu) Probed by NMR Spectroscopy and Quantum Chemical Calculations. *Inorg. Chem.* **2024**, *63*, 12969.
(95) Andreev, G.; Budantseva, N.; Sokolova, M.; Fedoseev, A. Perrhenate and Pertechnetate Complexes of U(IV), Np(IV), and Pu(IV) with Dimethyl Sulfoxide as an O-Donor Ligand. *Inorg. Chem.* **2020**, *59* (16), 11357−11365.
(96) Galley, S. S.; Pattenaude, S. A.; Gaggioli, C. A.; Qiao, Y.; Sperling, J. M.; Zeller, M.; Pakhira, S.; Mendoza-Cortes, J. L.; Schelter, E. J.; Albrecht-Schmitt, T. E.; et al. Synthesis and Characterization of Tris-Chelate Complexes for Understanding f-Orbital Bonding in Later Actinides. *J. Am. Chem. Soc.* **2019**, *141*, 2356.
(97) Whiting, C. E.; Du, M.; Felker, L. K.; Wham, R. M.; Barklay, C. D.; Kramer, D. P. Kinetics of the High Temperature Oxygen Exchange Reaction on $^{238}PuO_2$ Powder. *J. Nucl. Mater.* **2015**, *467*, 770−777.
(98) Sadergaski, L.; Andrews, H.; Miskowiec, A.; Abrecht, D.; Schrell, S. *Characterizing PuO_2 Powder at Oak Ridge National Laboratory for the Multi-Lab Plutonium Process Signatures Campaign FY 2022*, ORNL/TM--2023/2852, 1965242, 2023; p ORNL/TM-2023/2852, 1965242.
(99) *Nuclear Data Services - International Atomic Energy Agency*. https://www-nds.iaea.org/.
(100) Spek, A. L. Single-Crystal Structure Validation with the Program *PLATON*. *J. Appl. Crystallogr.* **2003**, *36* (1), 7−13.
(101) Sheldrick, G. M. SHELXT - Integrated Space-Group and Crystal Structure Determination. *Acta Crystallogr.* **2015**, *A71*, 3−8.
(102) Dolomanov, O. V.; Bourhis, L. J.; Gildea, R. J.; Howard, J. A. K.; Puschmann, H. OLEX2: A Complete Structure Solution, Refinement and Analysis Program. *J. Appl. Crystallogr.* **2009**, *42*, 339−341.
(103) Sheldrick, G. M. A Short History of SHELX. *Acta Crystallogr.* **2008**, *A64*, 112−122.
(104) Johnson, W.; Chan, E.; Walsh, E.; Morte, C.; Lee, D. *InterSpec v. 1.0.9*; Sandia National Lab (SNL-NM): Albuquerque, NM, United States, 2021.https://doi.org/10.11578/dc.20221016.3.
(105) DeVries, D.; Griffin, H. X- and *γ*-Ray Emissions Observed in the Decay of ^{237}Np and ^{233}Pa. *Appl. Radiat. Isot.* **2008**, *66* (5), 668−675.
(106) Varga, L. P.; Reisfeld, M. J.; Asprey, L. B. Electronic Spectra of the $5f^3$ Actinides: U^{3+}, Np^{4+}, Pu^{5+}, and AmO_2. The F^3 Intermediate Coupling Diagram. *J. Chem. Phys.* **1970**, *53* (1), 250−255.

https://doi.org/10.1021/acs.inorgchem.4c02099
Inorg. Chem. 2024, 63, 18417−18428